Supplemental Material

Transitions between spatial maps in place-cell networks

R. Monasson, S. Rosay

SIMULATIONS

Monte Carlo sampling of the Gibbs measure associated to energy E in Eq. (2) of the main text and at fixed temperature T is done with the fixed-activity constraint,

$$\sum_{i=1}^{N} \sigma_i = fN \ . \tag{1}$$

We start from a configuration that fulfills (1). At each time step we select uniformly at random one active neuron, say, $\sigma_i = 1$, and one silent neuron, say $\sigma_j = 0$. We compute the variation in energy ΔE resulting from the double flip $(\sigma_i = 1, \sigma_j = 0) \to (\sigma_i = 0, \sigma_j = 1)$, and apply Metropolis rule: the double flip is accepted if $\Delta E < 0$ or with probability $\exp(-\beta \Delta E)$ if $\Delta E \geq 0$, and rejected otherwise. This procedure ensures that the system converges to thermodynamic equilibrium at temperature $T = 1/\beta$ and fulfills constraint (1). To determine the environment in which the activity is localized we compute the contribution

$$E_\ell = -\sum_{i<j} J(|\vec{x}_{\pi^\ell(i)} - \vec{x}_{\pi^\ell(j)}|)\, \sigma_i\, \sigma_j \tag{2}$$

of each map ℓ to the total energy. The lowest value, if substantially smaller than the PM energy, identifies the retrieved environment. The center of the bump e.g. used to determine the initial and final locations in Fig. 5b of the main text is identified as follows. Space is discretized into bins of size roughly equal to the bump width, and the location of the center is defined as the index of the bin of maximal activity.

One-dimensional maps. We show in Fig. 1 the rates of transitions from one map to another found for network of various sizes N in the (α, T) plane, in the case of one-dimensional environments. The same data are plotted as a function of temperature, for various values of the size N and of the load α in Fig. 2. We observe that the transition rate increases with T and with α, and is a strongly (approximately, exponentially) decreasing function of the size N.

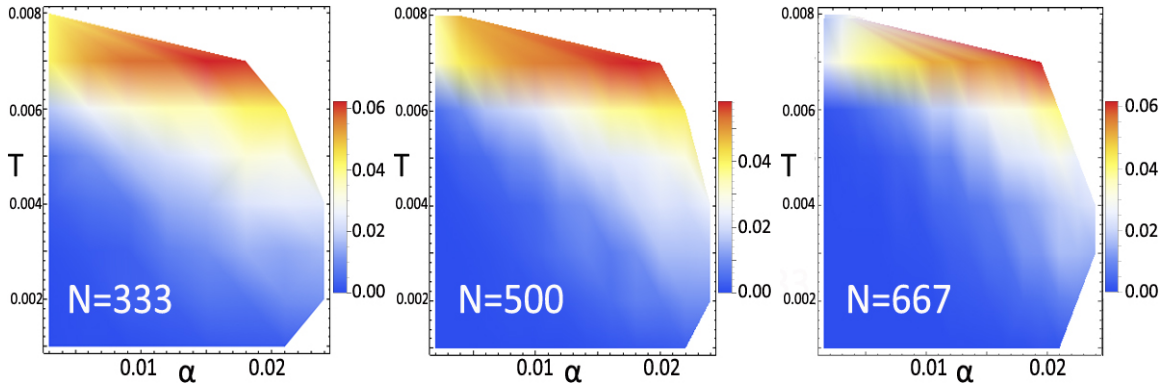

FIG. 1: Rate of transitions between maps as a function of α and T in the CL phase of the one-dimensional model with $L = 2$ maps. Rates have been estimated based on Monte Carlo simulations with $N = 333$ (left), $N = 500$ (center) and $N = 667$ units (right). Each point is averaged over 100 simulations of 10,000 rounds each (one round = N Monte Carlo steps). Note the decrease of the rate as N increases at fixed α, T. Parameter values: $f = 0.1, w = 0.05$. Maps are one-dimensional, with periodic boundary conditions.

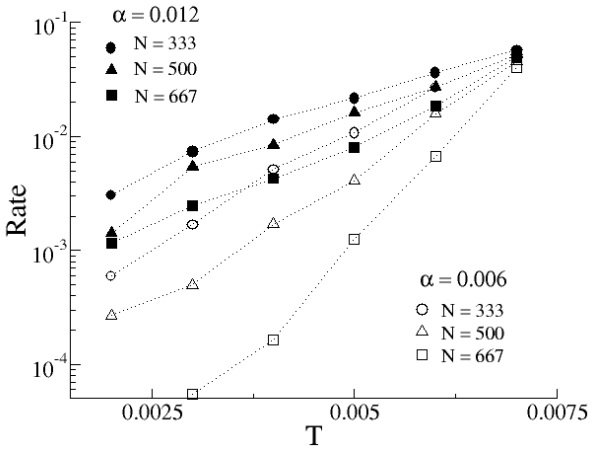

FIG. 2: Rate of transitions between maps as a function of the temperature T for two values of α and for three values of the size N. Same conditions as in Fig. 1.

Two-dimensional maps. The file '2Dsimulations.mp4' shows the outcome of Monte Carlo simulations with $L = 3$ two-dimensional maps and parameters $w = 0.2$, $f = 0.05$, $T = 0.004$, $N = 90 \times 90$, and a fraction $c = 0.6$ of cells having a place field in each map. The top and the bottom left panels represent the activity of the population in each one of the three maps. Dots locate the place-field centers of active neurons. The black cross shows the position of the center of mass of the bump in the map where the activity is localized. The bottom right panel shows the time evolution of the contributions to the energy associated to the three maps, rescaled by the energy in the PM phase. The sliding bar gives the value of the time. In the first part of the video, the activity is localized in map 1 and the bump diffuses within this map. We then observe a transition from map 1 to map 2, through a 2-bump transition state.

FREE ENERGY AND DENSITY PROFILES FOR A GIVEN SAMPLE

Given a sample (set of environments defined by the permutations π^ℓ), the free energy associated to the average neural activities $\{\rho_i = \langle \sigma_i \rangle\}$ reads

$$\mathcal{F}_\pi(\{\rho_i\}) = -\sum_{i<j} J_{ij}\,\rho_i\,\rho_j + T\sum_i \left[\rho_i \log \rho_i + (1-\rho_i)\log(1-\rho_i)\right] . \tag{3}$$

where the couplings J_{ij} are defined in Eq. (3) of the main text. This free energy is equal to the sum of the energetic contributions coming from the different environments, minus the entropy of the ρ_i-distribution multiplied by the temperature. We obtained the values of the average neural activities ρ_i upon minimization of $\mathcal{F}_\pi$.

A representative set of average activites ρ_i obtained upon minimization of $\mathcal{F}_\pi$ for parameters α, T corresponding to the CL phase is shown in Fig. 3(a). Despite the granularity due the quenched permutations, the localization of the activity profile in one map and the lack of coherence in the other map(s) clearly appears after coarse graining. We observe the presence of a smooth bump-like profile in the retrieved environment. Note that, while bumps can be translated without affecting the replicated free energy $\mathcal{F}$ in the CL phase this is not true for a given realization of the permutations and finite N. Due to the presence of the quenched disorder, the bump is anchored at a specific position in the retrieved map (Fig. 3(a)).

When the size N is small enough, repeated gradient descents of $\mathcal{F}_\pi$ from a large number of initial conditions may eventually end up in a local minimum $\{\rho_i\}$, partially localized in two maps, see Fig. 3(b), and with higher free energy than the global minimum CL (Fig. 3(a)). Such local minima are are less and less stable as N grows, in agreement with the saddle-point nature of TS_2.

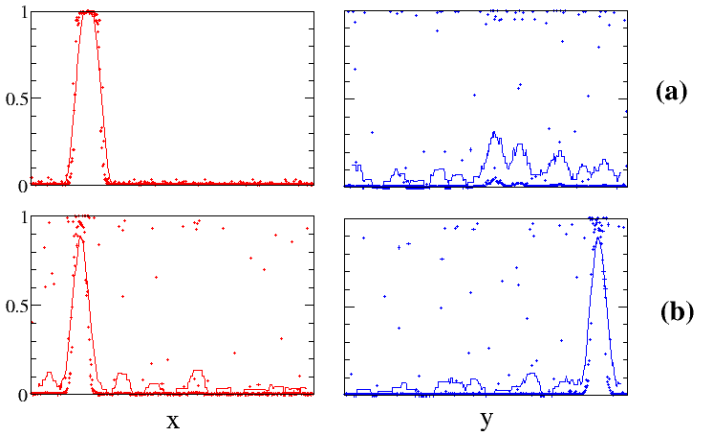

FIG. 3: **(a)** Average activities ρ_i (dots) in the minimum of $\mathcal{F}_\pi$ (3), corresponding to CL^A, for one random realization of the permutations π^A and π^B, and $T = 0.005$. Neurons $i = 1, ..., 600$ are sorted in increasing order of their place-field centers in A and B; the continuous lines show the running averages of ρ_i over 30 points. **(b)** average activities ρ_i (dots) and running averages over 30 points (continuous lines) in a local minimum of $\mathcal{F}_\pi$, similar to TS_2, for the same permutations π^A, π^B as in panel (a). Same parameter values as in Fig. 2 of the main text.

ROBUSTNESS TO HETEROGENEITIES IN THE COUPLING MATRIX

In order to be analytically tractable, the place cell model we study relies on several simplifying assumptions. Notably, the coupling matrix we consider in the model assumes that all environments are equally explored and covered by place fields, with all place cells having a place field in each environment – a hypothesis we know to be unrealistic. In this Section we check that the transitions scenarios found in our idealized model are also present when the hypothesis is relaxed. More precisely, we introduce heterogeneities in the coupling matrix in two ways, through the existence of 'silent cells', and through the presence of more than two maps that induce quenched noise in the couplings.

Silent cells. It has been observed experimentally that in a given environment, only a fraction of the place cells have place fields, the other cells being 'silent' [20]. We incorporate this fact in our model by introducing a dilution parameter c denoting the fraction of cells having place fields in any environment. We have shown in previous publications [9,19] that this modification does not induce qualitative changes in the phase diagram nor in the quasiparticle properties of the model. We report in Fig. 4 the results of Monte Carlo simulations with $c < 1$, which show that the transition properties are not qualitatively affected either.

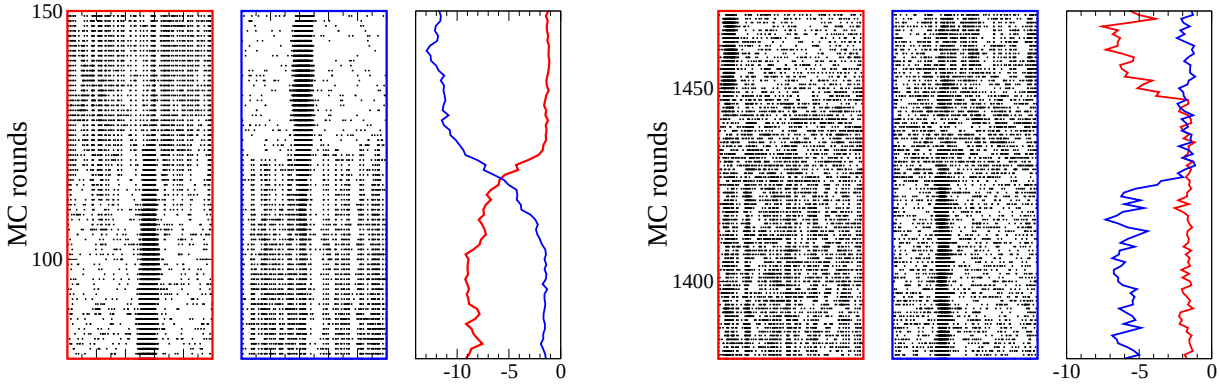

FIG. 4: Monte-Carlo simulations illustrating the transition scenarios in the presence of silent cells, and energy contributions due to each map in units of $f^2c^2w/2$ (absolute value of the PM energy). Left: TS_2-like transition. Right: TS_1-like transition. Parameter values: $N = 1000$, $c = 0.7$, $f = 0.1$, $w = 0.05$, $L = 2$, $T = 0.004$ (left) and $T = 0.006$ (right).

More maps. We have also looked at simulations with more than two maps. Here again, the two transition scenarios identified in our analytical solution of the idealized model are still observed. Figure 5 shows examples of TS_2 and of TS_1 scenarios, with delocalisation of the activity through the PM phase in the latter case. For parameter values such that the clump and the SG phases coexist, *i.e.* for intermediate values of the number of environments, TS_2 and TS_1 transitions are also observed, as shown in Fig. 6.

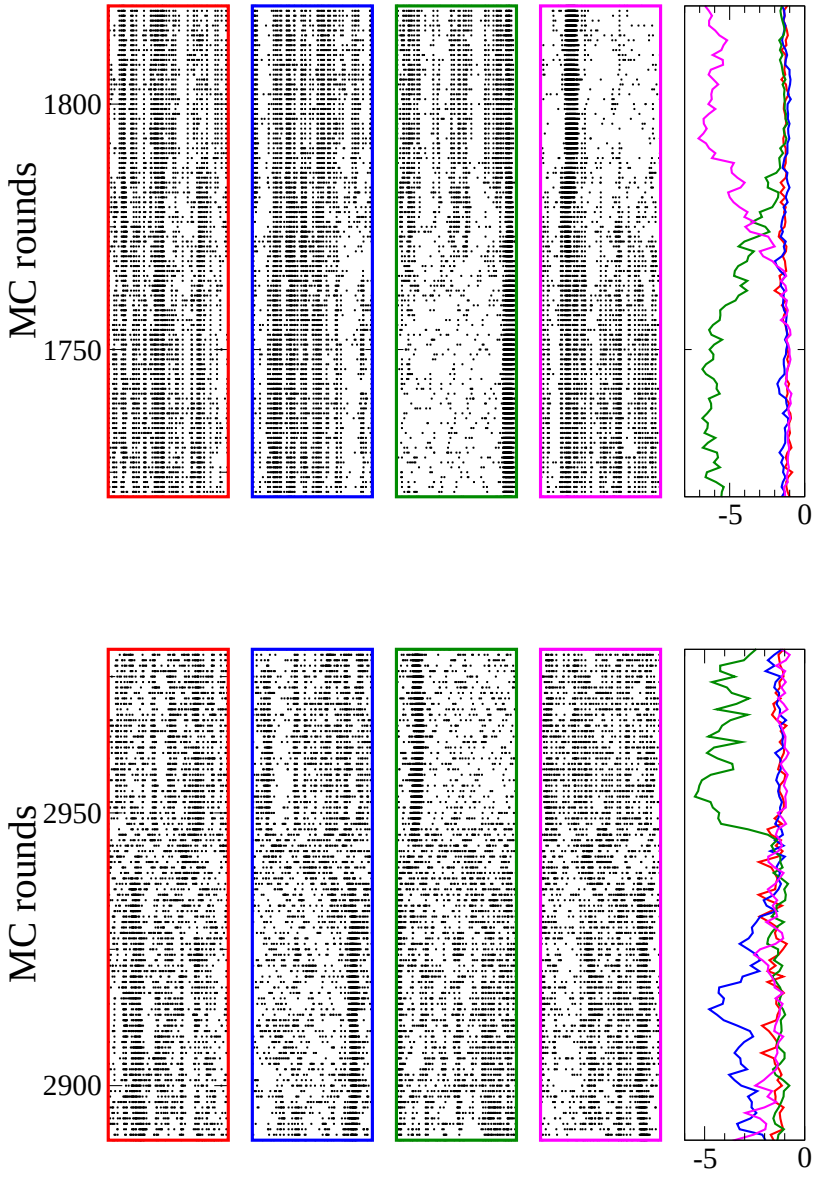

FIG. 5: Monte Carlo simulations illustrating the transition scenarios in the case of $L = 4$ environments, and energy contributions due to each map in units of $f^2w/2$ (absolute value of the PM energy). Top: TS_2-like transition. Bottom: TS_1-like transition, expected to take place through the PM phase. Parameter values: $N = 500$, $f = 0.1$, $w = 0.05$, $L = 4$, $T = 0.005$ (top) and $T = 0.0065$ (bottom).

As a conclusion, in both attempts to relax the unrealistic assumption about the homogeneity of the coupling matrix, we observe in the simulations the two transition scenarios, based on TS_1, TS_2 found by analytical resolution of the homogeneous model. We expect the two transition scenarios to hold also in the presence of other sources of noise,

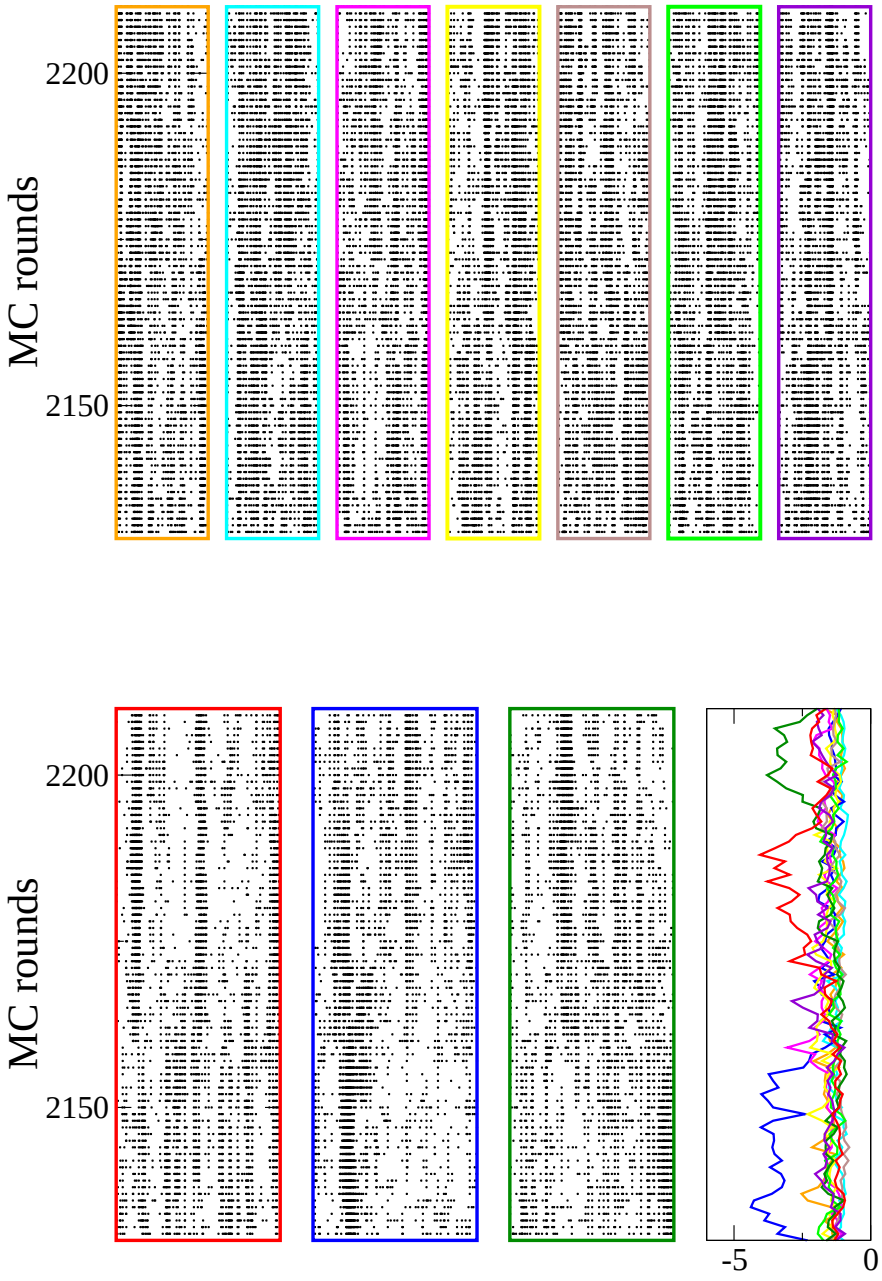

FIG. 6: Monte Carlo simulations illustrating the transition scenarios in the case of $L = 10$ environments, and energy contributions due to each map in units of $f^2w/2$ (absolute value of the PM energy). Both TS_1-like (expected to take place through the SG phase) and TS_2-like transitions are observed, around, respectively $t \approx 2160$ MC rounds and $t \approx 2190$ MC rounds. Bottom-row panels show the activity in the tree maps where it is alternatively localized over time, while the top row corresponds to the remains seven maps. Parameter values: $N = 500$, $f = 0.1$, $w = 0.05$, $L = 10$, $T = 0.006$.

such as uneven exploration of the environment, randomness in the place field centers (instead of a regular grid)..., which are not believed to lead to a fundamentally different model to the one with $c < 1$ or $\alpha > 0$, as discussed in [9]. Varying the degree of the couplings or the relative weight of environments is likely to favor certain positions over others and quantitatively change the frequency of transitions, but no qualitative change is expected.

NUMERICAL SOLUTION OF THE SADDLE-POINT EQUATIONS FOR THE REPLICA-SYMMETRIC FREE ENERGY

We explain the procedure followed to find the saddle-point solutions of the replica symmetric free energy $\mathcal{F}$. Space is first discretized into $2n+1$ bins, $b = 1, 2, \dots 2n+1$. The free-energy functional $\mathcal{F}$ is then a function of the density profiles $\{\rho_b\}$ and of the conjugated forces $\{\mu_b\}$ in each map, and of the Edwards-Anderson overlap q and of its conjugated force r; η in Eqn. (3) of the main text is determined to fulfill constraint (1) and is not an independent parameter. The total number of arguments of $\mathcal{F}$ is therefore $\mathcal{D} \equiv 4 \times (2n+1) + 2 = 8n + 6$. The number n of bins is often chosen to be 100 or 200 in practice.

We write the saddle-point equations for $\mathcal{F}$, Eq. (3) of the main text, as follows:

$$\rho^A(\vec{x}) = V^A(\{\rho^A, \rho^B\}, q; \vec{x}) \ , \quad \rho^B(\vec{y}) = V^B(\{\rho^A, \rho^B\}, q; \vec{y}) \ , \quad q = W(\{\rho^A, \rho^B\}, q) \ , \tag{4}$$

where

$$\begin{aligned} V^A(\{\rho^A, \rho^B\}, q; \vec{x}) &= \int d\vec{y}\, Dz\ m(\{\rho^A, \rho^B\}, q; \vec{x}, \vec{y}, z) \ , \\ V^B(\{\rho^A, \rho^B\}, q; \vec{y}) &= \int d\vec{x}\, Dz\ m(\{\rho^A, \rho^B\}, q; \vec{x}, \vec{y}, z) \ , \\ W(\{\rho^A, \rho^B\}, q) &= \int d\vec{x}\, d\vec{y}\, Dz\ m(\{\rho^A, \rho^B\}, q; \vec{x}, \vec{y}, z)^2 \ , \end{aligned} \tag{5}$$

and

$$\begin{aligned} m(\{\rho^A, \rho^B\}, q; \vec{x}, \vec{y}, z) &= \frac{1}{1 + \exp\big(-\beta \big[\mu^A(\{\rho^A, \rho^B\}, q; \vec{x}) + \mu^B(\{\rho^A, \rho^B\}, q; \vec{y}) + z\sqrt{\alpha\, r(q)} - \eta \big] \big)} \ , \\ \mu^A(\{\rho^A, \rho^B\}, q; \vec{x}) &= \int d\vec{x}'\, J(\vec{x} - \vec{x}')\, \rho^A(\vec{x}') \ , \quad \mu^B(\{\rho^A, \rho^B\}, q; \vec{y}) = \int d\vec{y}'\, J(\vec{y} - \vec{y}')\, \rho^A(\vec{y}') \ , \\ r(q) &= 2(q - f^2) \sum_{\vec{k} \neq \vec{0}} \left(\frac{1}{\Lambda_{\vec{k}}} - \beta(f - q) \right)^{-2} \ , \end{aligned} \tag{6}$$

and the eigenvalues $\Lambda_{\vec{k}}$ of the coupling matrix J are given in the main text. In addition to the saddle-point equations (4) the value of η is computed such that the average activity in either map is equal to f:

$$f = \int d\vec{x}\, d\vec{y}\, Dz\ m(\{\rho^A, \rho^B\}, q; \vec{x}, \vec{y}, z) \ . \tag{7}$$

We find five classes of solutions for the saddle-point equations (Figs. 2 and 3 of the main text):

- the delocalized paramagnetic (PM) solution: $\rho^A(x) = \rho^B(y) = f, q = f^2$. This solution is found at high temperatures T and small loads α.
- the delocalized spin glass (SG) solution: $\rho^A(x) = \rho^B(y) = f, q > f^2$. This solution is found at low temperatures T and large loads α.
- the single-environment localized (clump, CL) solution: $\rho^A(x)$ localized in space, $\rho^B(y) = f$ (state CL^A) or vice-versa (state CL^B). This solution is stable at low temperature, and unstable at high temperature.
- the two-environment transition state (TS_2): $\rho^A(x) = \rho^B(x)$ localized in space, but less strongly than in the CL state, and neurons outside the bump have larger, fluctuating activities. The TS_2 solution is unstable with respect to a small asymmetric perturbation of the densities ρ^A and ρ^B.
- the one-environment transition state (TS_1): $\rho^A(x)$ is localized in space, but less strongly than in the CL state, and $\rho^B(x) = f$. The TS_1 solution is unstable with respect to a small perturbation of the density ρ^A. TS_1 may be found only for values of T and α such that the CL and the PM (or the SG) solutions coexist.

To determine the transition-state solution TS_2 we simply iterate the saddle-point equations (4) with the constraint $\rho^A = \rho^B$ at any iteration t, until a fixed point is found. This solution is a minimum in the constrained subspace, and is unstable against any perturbation such that $\rho^A \neq \rho^B$.

It is harder to determine TS_1 for fixed α and T. To do so we iterate the saddle-point equations (4), starting from

$$\rho^A(x, t = 0) = (1 - z)\, f + z\, \rho^{CL}(x) \ , \tag{8}$$

and $\rho^B(y, t = 0) = f$. Here, $\rho^{CL}(x)$ is the profile of activity for the CL phase, and z is an arbitrary coefficient chosen in the $[0; 1]$ range. After many iterations convergence is reached for ρ^A ($\rho^B = f$ is a fixed point), either towards the PM or SG (for sufficiently low values of z) or the CL (for sufficiently large z) solution. The separatrix between the basins of attractions of the two solutions corresponds to a 'critical' value of z, see Fig. 7(a). When z is close to this critical value, $\rho^A(x, t)$ gets close to the desired unstable fixed-point TS_1 for many iterations, until it eventually falls into one of the two basins (Fig. 7(a)). As a consequence the free energy $\mathcal{F}$, Eq. (3) of the main text, computed for $\rho^A(x, t), \rho^B = f$ shows a plateau behaviour, see Fig. 7(b). The height of the plateau is our estimate for the free energy of the transition state TS_1.

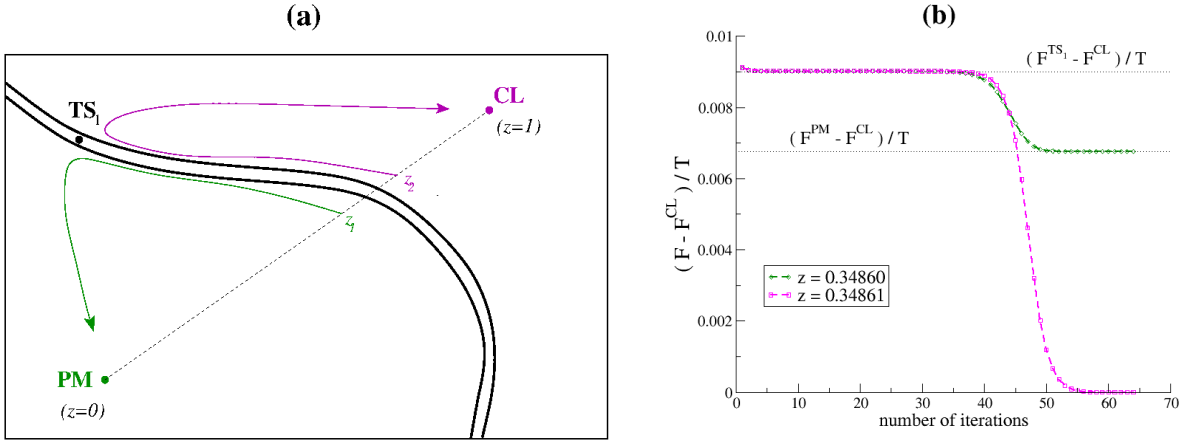

FIG. 7: **(a)** Sketch of the $\mathcal{D}$–dimensional space of order parameters. The representative points of the PM and CL phases are local minima of the free-energy functional $\mathcal{F}$, see Eq. (3) of the main text. The $(\mathcal{D} - 1)$–dimensional separatrix between the basins of attraction of the PM and CL fixed points, solutions of (4), is symbolised by the double line. The transition state TS_1 lies in this manifold. We interpolate between the PM and the CL phases through a linear relation parametrized by $z \in [0; 1]$, see (8). This line cut the separatrix for a critical value of z. Choosing z_1 and z_2 slightly off the critical value leads to either PM or CL. In both cases the flow spends a long time (number of iterations) close to TS_1, which allows us to measure the value of its free energy with accuracy. **(b)** Free energy as a function of the number t of iterations for the density $\rho^A(x, t)$, and for two close values of z, see legend, on opposite sides of the separatrix. We observe the plateau behaviour corresponding to TS_1 for intermediate values of t, prior to the convergence to the PM (green) or the CL (magenta) activity profile. Parameter values: $T = 0.007$, $\alpha = 0$.